Materials and Design 188 (2020) 108414

Contents lists available at ScienceDirect

Materials and Design

journal homepage: www.elsevier.com/locate/matdes

Design of FDM 3D printed polymers: An experimental-modelling methodology for the prediction of mechanical properties

S. Garzon-Hernandez[a,*], D. Garcia-Gonzalez[a], A. Jérusalem[b], A. Arias[a]

[a]Department of Continuum Mechanics and Structural Analysis, University Carlos III of Madrid, Avda. de la Universidad 30, Leganés 28911, Madrid, Spain
[b]Department of Engineering Science, University of Oxford, Parks Road, Oxford OX1 3PJ, UK

HIGHLIGHTS

- FDM ABS specimens are tested for different combinations of printing parameters.
- A two-stage model is proposed to simulate the FDM manufacturing process.
- The model predicts thermal conditions and sintering within filaments.
- Analytical expressions are established for FDM ABS.
- Layer height and environment temperature main drivers for mechanical properties.

GRAPHICAL ABSTRACT

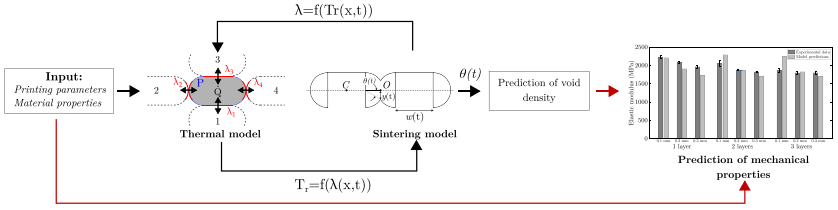

ARTICLE INFO

Article history:
Received 4 October 2019
Received in revised form 5 December 2019
Accepted 7 December 2019
Available online 24 December 2019

Keywords:
Fused deposition modelling (FDM)
Additive manufacturing
3D printing
Thermoplastic polymers
Sintering
Mechanical properties

ABSTRACT

Additive manufacturing technologies provide new opportunities for the manufacturing of components with customisable geometries and mechanical properties. In particular, fused deposition modelling (FDM) allows for customisable mechanical properties by controlling the void density and filament orientation. In this work, a methodology is provided for the prediction of the mechanical properties and mesostructure of FDM polymers. To this end, we propose a computational framework for the simulation of the printing process taking as input data specific manufacturing parameters and filament properties. A new two-stage thermal and sintering model is developed to predict the bond formation process between filaments. The model predictions are validated against original experimental data for acrylonitrile butadiene styrene (ABS) components manufactured by FDM. A parametric study is finally presented to interpret the effects of different manufacturing parameters on the mechanical performance of ABS specimens. Overall, the proposed framework offers new avenues for the design of 3D printed polymeric components with custom properties, directly in terms of manufacturing settings.

1. Introduction

Fused deposition modelling (FDM) is one of the most widely used additive manufacturing techniques for rapid prototyping and composites components design due to its simplicity, high speed and low cost [1]. FDM components present inferior mechanical properties compared with other traditional techniques due to the porosity arising from the printing process. In addition, a marked anisotropic behaviour is observed in FDM components, which is defined by the raster orientation [1]. However, higher porosities can be an advantage in some applications such as scaffold design in tissue engineering [1]. Moreover, FDM provides customisability of the mechanical properties by controlling the void density and filament orientation. In addition, new 4D printing possibilities have been proposed to introduce functional

* Corresponding author.
E-mail addresses: sgarzon@ing.uc3m.es (S. Garzon-Hernandez), danigarc@ing.uc3m.es (D. Garcia-Gonzalez), antoine.jerusalem@eng.ox.ac.uk (A. Jérusalem), aariash@ing.uc3m.es (A. Arias).

https://doi.org/10.1016/j.matdes.2019.108414

responses in polymeric structures [2, 3]. Overall, FDM is a complex process with a large number of parameters that influence the quality and properties of the components [4].

At the macroscopic level, the structure of the FDM components is composed of layers bonded together [5]. Each layer is composed of polymeric filaments (rasters) partially bonded, and voids [5]. The mechanical properties of FDM components are determined by the material properties of the filaments, the void density and the fibre-to-fibre bond strength. Void density and bond strength are, in turn, determined by the bonding process between adjacent filaments that take place during printing and, therefore, are influenced by the printing and process parameters.

With the aim to understand the thermodynamics of the printing process, some authors have modelled the bonding process during 3D printing, obtaining the final geometry of the filaments as a function of the printing parameters. Bonding is a process driven by the thermal energy of the semi-molten material [5-7]. The formation and quality of the bond depends on the neck growth, described by sintering, and the molecular diffusion reached within it, see Fig. 1. Sintering is the phenomenon involving the coalescence of particles and is driven by two temperature-dependent properties: surface tension and viscosity [8, 9]. To achieve a complete coalescence between filaments, it is necessary to lower the viscosity sufficiently to enhance the flow of the material. However, sometimes lower viscosities are not possible without inducing thermal damage [10] and, therefore, the bonding between filaments is not perfect, leading to the formation of voids between rasters. In this regard, Bellehumeur et al. [5] and Sun et al. [7] proposed a methodology to study the printing parameters influence on the degree of bonding. To this end, both references combined a thermal analysis of the FDM process, from which the temperature profile of the filaments was predicted, with the sintering model proposed by Pokluda et al. [9].

In parallel to these efforts, several authors have proposed models to predict the mechanical properties as a function of void ratio. Li et al. [11] proposed a set of equations to determine the elastic constants of FDM components where the void ratio is estimated from analytical expressions based on the cross-sectional geometry of the filaments. Rodriguez et al. [12] developed a mathematical model to optimise the mechanical performance of a component taking as input data the geometry and void ratio. Although both efforts provide potential tools for the optimisation of mechanical properties, previous experimental measurements are needed as model inputs.

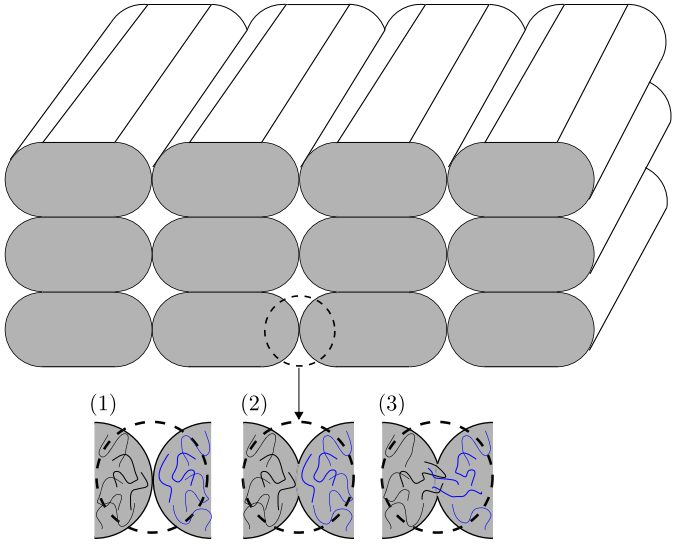

Fig. 1. Bond formation process through sintering: (1) surface contact; (2) neck growth; (3) neck growth and molecular diffusion at the interface.

Parametric approaches for the identification of the mechanical properties of FDM components have also been carried out. In this regard, Sood and coworkers have developed empirical models relating mechanical properties and printing parameters based on central composite design [13, 14]. However, these models do not link mechanical properties with physical variables and are restricted to specific printing parameters.

Therefore, models allowing for the simulation of the bonding process during FDM printing are needed to provide estimations of the structural and mechanical properties of the printed components. In this work, a methodology is proposed for the prediction of the mechanical properties of FDM polymers as a function of the void density, raster orientation, and number of layers, taking as input data manufacturing and material parameters, see Fig. 2.

This work is structured as follows: Section 2 introduces a mechanical and mesostructural characterisation of FDM components as a function of printing parameters, using acrylonitrile butadiene styrene (ABS) material. Building on these experimental observations, Section 3 introduces a two-stage thermo-structural model aimed at predicting the final mesostructure of the filaments during the printing process. Theoretical expressions for the prediction of the void density and mechanical properties are described and validated in Section 4. This methodology is then used for the prediction of the mesostructural and mechanical properties of FDM components through end-to-end simulations of the printing process in Section 5. Finally, the model is leveraged to establish the influence of the manufacturing parameters on the mechanical performance of FDM polymers.

2. Experimental characterisation of FDM polymers

Several authors have studied the influence of printing parameters on the mechanical properties and void density of FDM components [4, 10, 13, 15-21]. In particular, layer height and raster orientation have been found of great importance [13, 19]. Higher elastic modulus and yield stress are observed for lower layer height [17]. This improvement is accompanied by a decrease in the void density. Specimens manufactured with a raster orientation of 0° (longitudinal) with respect to the loading direction present the highest tensile performance as the molecules tend to align along the stress axis direction [20]. On the contrary, specimens manufactured with a raster angle of 90° (transverse) present the lowest tensile performance, since the loads are taken by the bond between filaments and not by the filaments themselves [20].

In addition, the number of layers has also been identified as a key parameter in the determination of the final mechanical properties. A higher number of layers results in a higher temperature gradient in the first layers. This leads to an increase in the diffusion process between adjacent rasters, decreasing the void ratio and improving the strength of the bond [13]. However, this can also lead to a greater number of heating and cooling cycles and, therefore, can increase the residual stress.

This section summarises the experimental program of this work, whose main goal is the interpretation of the influence of layer height, raster orientation and number of layers on the mesostructural and mechanical behaviour of FDM ABS. Further details on the material and manufacturing process of the specimens, as well as on the experimental methods used, are provided in *Supplementary Information* (*Sections S1 and S2*).

2.1. Void density and cross-sectional geometry dependencies on manufacturing parameters

Two sets of specimens were tested: (i) two-layer specimens with layer heights of 0.2 and 0.3 mm; (ii) 1.2 mm thickness specimens with layer heights of 0.1, 0.2 and 0.3 mm. An analysis of the samples was performed by means of micrographs of the cross-section using

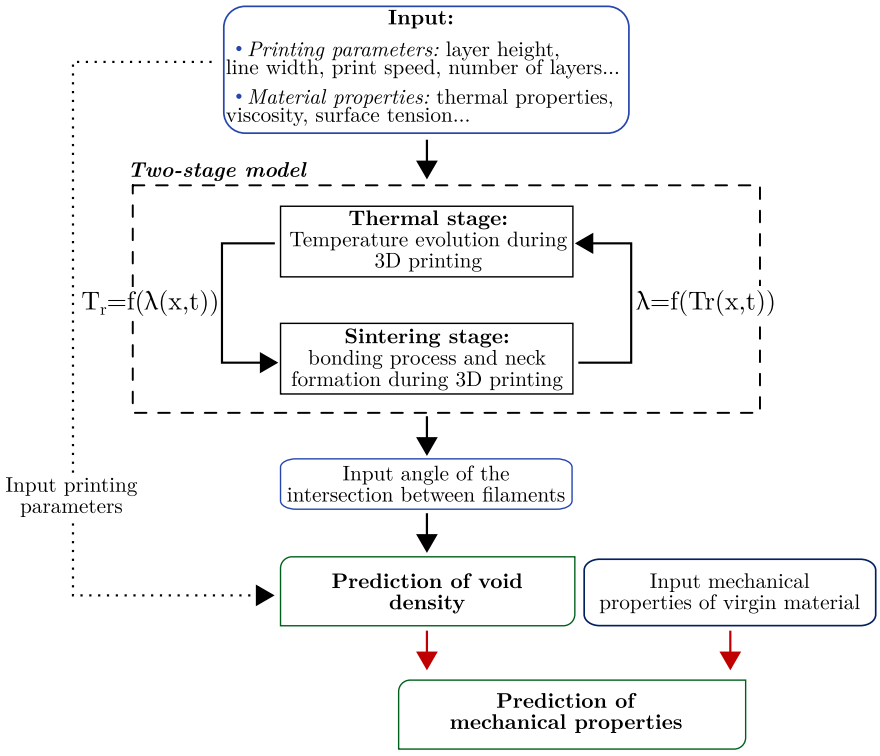

Fig. 2. Procedure to estimate structural and mechanical properties of FDM components.

a Scanning Electron Microscope. The resulting micrographs for the second test are shown in Fig. 3 (the micrographs for the two-layer specimens can be found in *Supplementary Information, Fig. S1*).

Although the material is extruded through a circular nozzle, during the deposition, the flow of material is limited by the platform or the previous layer deposited underneath and by the extruder above, which also applies pressure during its movement (see *Supplementary Information, Fig. S2*). The cross-section of a filament after the deposition can thus be modelled, as a first approximation, as two half-discs and a rectangle. In this regard, the cross-sectional geometry is mainly determined by the layer height and the line width (see Fig. 3c).

The void density of the different specimens was measured using ImageJ software [22]. The void density is taken as the ratio of the total area of voids to the cross-sectional area. Note that, since the length of the filaments is the same as the voids', the void density is equivalent to porosity. In the case of the specimens with a thickness of 1.2 mm, the measurements were made excluding approximately 0.4 mm of the specimen bottom thickness due to defects associated with 3D printer bed levelling, showing that the void density increases with the layer height (see *Supplementary Information, Table S2*). Although the void density of transverse specimens is greater, these specimens are not completely aligned due to manufacturing defects. This skewed mesostructure causes the appearance of small voids at the contact point between the top and bottom fibres leading to a slight increase in void density. Moreover, comparing results of the two-layer specimens to the specimens with a thickness of 1.2 mm, the values of void density are similar for each layer height. As a conclusion, the void density is highly influenced by geometrical printing parameters such as the layer height and line width.

2.2. Mechanical dependencies on manufacturing parameters

This section studies the influence of layer height, raster orientation and number of layers on the mechanical properties of FDM polymers. To study the influence of the number of layers, specimens made of one, two and three layers were manufactured. The results can be found in *Supplementary Information* (*Table S3*), where the maximum stress corresponds to the yield stress in the case of longitudinal specimens and to the ultimate tensile strengths in the case of transverse specimens.

Longitudinal specimens show higher elastic modulus and maximum stress compared to transverse. Moreover, the comparison of different layer heights shows that the elastic modulus and maximum stress decrease by up to 8% and 14%, respectively, when the layer height increases from 0.1 mm to 0.2 mm. Furthermore, when the layer height increases from 0.2 mm to 0.3 mm, the elastic modulus and maximum stress decrease by up to 6% and 4%, respectively. These differences increase by up to 18% for transverse specimens. These tendencies are explained by the mesostructural characterisation, that shows an increase in void density with layer height. Similarly, the elastic modulus and maximum stress decrease by up to 10% and 4% when a new layer is added, for longitudinal specimens. However, an increase in the maximum stress by up to 25% is observed when the number of layers increases for transverse specimens.

3. Modelling of bond formation between filaments

This section describes the coupled two-stage model used to simulate the bond formation between filaments during 3D printing process (see the dashed line box in Fig. 2). To this end, an algorithm is proposed for the thermal model, based on the work by Costa et al. [23], to predict the temperature evolution of the filaments depending on the printing and material parameters. The predicted evolution of temperature can then be used as input for a new sintering model that describes the coalescence of adjacent filaments, providing the mesostructural details of the final printed component. This model extends the work by Pokluda et al. [9] and is governed by two material properties: temperature-dependent viscosity and surface tension.

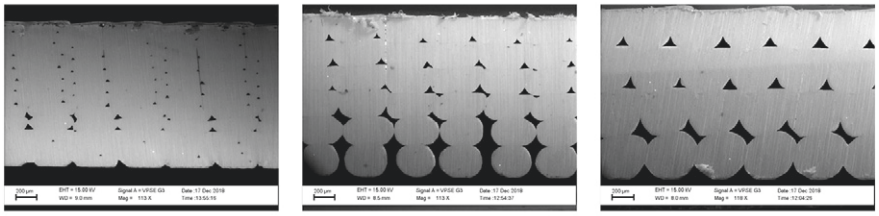

(a) (b) (c)

Fig. 3. Micrographs of the cross-sectional area of FDM structures with total thickness of 1.2 mm: (a) layer heights of 0.1 mm, (b) 0.2 mm and (c) 0.3 mm.

3.1. Thermal evolution during the 3D printing process

The temperature evolution of filaments during the 3D printing process depends on thermal conditions such as environment, platform and extrusion temperatures, as well as material properties and printing parameters such as print speed or those that define the cross-sectional area. In this regard, Thomas and Rodriguez [24] carried out a 2D transient heat transfer analysis applied to a filament deposited on a vertical stack. However, this model assumes a rectangular cross-section and does not account for contacts between filaments. Other authors have used the lumped-heat-capacity method to interpret the cooling process of a single filament [5, 7] assuming that its diameter is relatively small and, therefore, modelling the cooling process as a 1D problem. Recently, Costa et al. [23] proposed a new analytical solution for the transient heat conduction during the printing process in FDM techniques. The boundary conditions considered are the contacts between filaments, between a filament and the support, and the heat transfer with the environment. Thus, once the filament is deposited, heat exchange occurs by convection with the environment and by conduction with the support and adjacent filaments. Considering a filament segment of length dx, the resulting equation can be rewritten as

$$\rho CA\frac{\partial T_r(x,t)}{\partial t}dx = -\left(h_{conv}A_{rconv}(T_r(x,t)-T_E)+\sum_{i=1}^{n}h_iA_{ri}(T_r(x,t)-T_{ri}(t))\right) \tag{1}$$

where the axial heat conduction has been neglected due to the low thermal conductivity of most polymers, the small cross-section of the extruded filaments and the small thermal gradient along the axial direction [25]. A more detailed description of this equation and its derivation can be found in the work by Costa et al. [23]. In addition, the definition of the variables used in Eq. (1) along with other relevant model variables are summarised in Table 1.

The area of filament in contact with the filament r or with the support can be expressed as a function of the fraction λ_i of the total perimeter P as

$$A_{ri} = Pa_{ri}\lambda_i dx \tag{2}$$

where $i \in \{1,\dots,n\}$ is each one of the contacts expressed in local numbering as shown in Fig. 4.

Similarly, the area exposed to the environment can be expressed by means of the total perimeter P as

$$A_{rconv} = P\left(1-\sum_{i=1}^{n}a_{ri}\lambda_i\right)dx \tag{3}$$

where the variable a_{ri} takes 1 if the filament segment r is in contact with another filament segment or with the support, and 0 otherwise; and n is the total number of physical contacts with other filaments. For simplicity in this work, we assume that $n \leq 4$. Taking Eq. (3) and using the characteristic polynomial method [26], the analytical solution for the time evolution of the filament temperature reads

$$T_r(x,t) = C_1 e^{\left[\frac{-Pb(a_{r1},\dots,a_{rn})}{\rho CA}(t-t_r(x))\right]} + Q(a_{r1},\dots,a_{rn}) \tag{4}$$

where $t_r(x)$ is the time at which each filament segment is deposited, the terms $b(a_{r1},\dots,a_{rn})$ and $Q(a_{r1},\dots,a_{rn})$ are functions that depend on the existing contacts:

$$b(a_{r1},\dots,a_{rn}) = \underbrace{h_{conv}\left(1-\sum_{i=1}^{n}a_{ri}\lambda_i\right)}_{K_1} + \underbrace{\sum_{i=1}^{n}a_{ri}h_i\lambda_i}_{K_2} \tag{5}$$

$$Q(a_{r1},\dots,a_{rn}) = \frac{h_{conv}(1-\sum_{i=1}^{n}a_{ri}\lambda_i)T_E + \sum_{i=1}^{n}a_{ri}h_i\lambda_i T_{ri}(t)}{b(a_{r1},\dots,a_{rn})} \tag{6}$$

and the term C_1 is defined as

$$C_1 = T_{extr} - Q(a_{r1},\dots,a_{rn}) \tag{7}$$

where T_{extr} is the extrusion temperature.

In the original work by Costa et al. [23], the algorithm implementation includes an iterative process to calculate the temperature when two filaments are in contact. In this paper, the formulation is rewritten in order to solve implicitly all temperatures at the same time to avoid the iterative process. To this end, we take dx to spatially discretise each filament in m segments. Here, Eq. (5) is divided into two terms where the first term K_1 defines the heat transfer by convection with the environment per unit temperature, while the second term K_2 defines the heat transfer by conduction between adjacent filament or support per unit temperature.

Combining Eqs. (4), (7) and (5), the evolution of filament temperature can be expressed as

$$T_r(x,t) - \frac{\sum_{j=1}^{m}a_{rj}h_j\lambda_j T_{rj}(t)}{K_1+K_2}\left[1-e^{\beta(t-t_r(x))}\right] = T_{extr}e^{\beta(t-t_r(x))} + \frac{K_1T_E}{K_1+K_2}\left[1-e^{\beta(t-t_r(x))}\right] + \frac{a_{rsupp}\lambda_1 h_{supp}T_{supp}}{K_1+K_2}\left[1-e^{\beta(t-t_r(x))}\right] \tag{8}$$

where $\beta = \frac{-P(K_1+K_2)}{\rho CA}$, T_{supp} is the support temperature, h_{supp} is the heat transfer coefficient between filament segment and support, λ_{supp} is the fraction of the perimeter in contact with the support, and a_{rsupp} is a variable that takes 1 if there is contact between the filament

Table 1
Nomenclature of the thermal model.

Nomenclature	
$T_r(x,t)$	Temperature at localisation x and time t of a given filament r (°C)
$T_{ri}(t)$	Temperature of the filament or support i in contact with the filament r at time t (°C)
T_E	Environment temperature (°C)
T_{supp}	Support temperature (°C)
T_{extr}	Extrusion temperature (°C)
$t_r(x)$	Time at which filament segment x of the filament r is deposited (s)
P	Perimeter of the cross-section (m)
A	Cross-sectional area (m^2)
A_{rconv}	Area exposed to the environment for filament r (m^2)
A_{ri}	Area of contact i for filament r (m^2)
dx	Filament segment length (m)
h_{conv}	Convective heat transfer coefficient (W/m^2°C)
h_i	Heat transfer coefficient of contact i (W/m^2°C)
C	Specific heat capacity (J/kg °C)
ρ	Density (kg/m^3)
n	Number of physical contacts with adjacent filament segment or support

element and the support, and 0 otherwise. Ultimately, the expression in its tensorial form reads as a linear system of the form

$$\boldsymbol{A}\cdot\boldsymbol{T} = \boldsymbol{B} \tag{9}$$

where A_{mm} and B_{m1} are all the temperature-dependent and -independent, respectively, terms of Eq. (8), and T_{m1} is the temperature at each point. Note that Eq. (9) is defined for each time increment.

3.2. Thermodynamics of the sintering process

Sintering is defined as the coalescence of particles under the action of surface tension [8, 9]. This process takes place at temperatures above glass transition T_g when the material is in a viscous or rubbery state. However, experimental observations suggest that most of the neck growth occurs during the first stage of the process, at temperatures above a critical sintering temperature (about 200 °C for ABS) [5, 6]. Thus, the evolution of the temperature plays a crucial role in the determination of the final mesostructure and quality of the printed components.

In the case of amorphous polymers, such as ABS, experimental studies have led to the conclusion that the sintering mechanism is essentially a Newtonian viscous flow where surface tension is the main driving force [27]. In this regard, different analytical models have been proposed in the literature to predict the rate of polymer sintering [9, 28-30]. Pokluda et al. [9] developed an analytical sintering model to describe the coalescence between two spherical particles based on the work balance of surface tension and viscous dissipation, where all other forces, including gravity, are neglected. Although the model has been used to describe the sintering process during FDM processes [5, 7], this approach presents important limitations related to the geometry of the filament cross-section. In this paper, we propose a new model based on the methodology proposed by Pokluda et al. [9] but considering realistic geometry based on experimental observations (see *Supplementary Information, Fig. S2*).

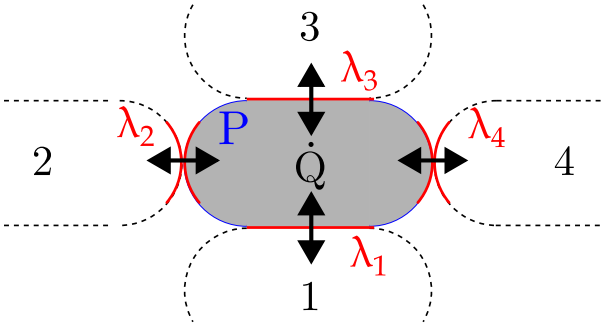

Fig. 4. Contact areas and heat flows of a single element.

Fig. 5 describes an idealised sintering process occurring during FDM where the layer height H_0 and length of each filament are assumed constant during the process. At initial time $t = 0$, the cross-section geometry is composed of two half-discs with a radius equal to $\frac{H_0}{2}$ and a rectangle with an initial width w_0 (this width is referred to as "line flat" in *Fig.S2*). At this point in time, there is only one contact point between the two filaments. With the evolution of the process, the centres of the contacting half-discs move towards the initial contact point O, producing the intersection of both half-discs, where $\theta(t)$ is the angle of the intersection and $y(t)$ is the radius of the neck (see Fig. 5).

In addition, $w(t)$ evolves with time so that conservation of mass is satisfied during the sintering process. The complete mathematical formulation of the sintering model can be found in the *Supplementary Information* (*Section S3*). The evolution of the angle of the intersection is obtained from a work balance of surface tension and viscous dissipation, where all the other forces are neglected.

The work of surface tension is defined as

$$W_s = -\Gamma(T_r(x,t))\frac{dS}{dt} \tag{10}$$

where $\Gamma(T_r(x,t))$ is the temperature-dependent coefficient of surface tension and S the surface of the system. Therefore, the resulting work of surface tension is obtained as

$$W_s = \Gamma(T_r(x,t))H_0L_0\,(\cos(2\theta)+1)\,\frac{d\theta}{dt} \tag{11}$$

On the other hand, considering a Newtonian fluid, the work of viscous forces is expressed as

$$W_v = \iiint_V \eta(T_r(x,t))\nabla\dot{\mathbf{u}} : (\nabla\dot{\mathbf{u}} + \nabla\dot{\mathbf{u}}^T)dV \tag{12}$$

where $\nabla\dot{\mathbf{u}}$ is defined as the spatial gradient of the velocity vector field, V is the volume of the system and $\eta(T_r(x,t))$ is the temperature-dependent coefficient of viscosity.

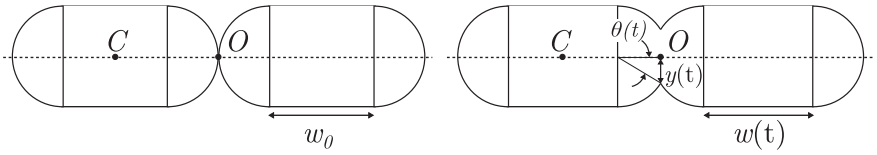

Fig. 5. Shape evolution during sintering.

Consequently, the dissipated energy reads

$$W_v = 4\eta(T_r(x,t))\left(\pi\left(\frac{H_0}{2}\right)^2 + H_0 w_0\right) \times L_0\left(\frac{-\frac{H_0}{2}\sin(\theta(t)) + \frac{H_0}{8} - \frac{H_0\cos(2\theta(t))}{8}}{\frac{H_0}{2}+\frac{w_0}{2}}\right)^2 \frac{d^2\theta(t)}{dt^2} \quad (13)$$

Finally, the evolution of $\theta(t)$ is obtained by equating the work of surface tension to the viscous dissipation. This derivation of $\theta(t)$ assumes that the variation of the angle of the intersection with time is always positive, so that

$$\frac{d\theta(t)}{dt} = \frac{\Gamma(T_r(x,t))H_0}{4\eta(T_r(x,t))} \frac{2\cos(\theta(t))^2}{\left(\pi\left(\frac{H_0}{2}\right)^2 + H_0 w_0\right)\left(\frac{-\frac{H_0}{2}\sin(\theta(t)) + \frac{H_0}{8} - \frac{H_0\cos(2\theta(t))}{8}}{\frac{H_0}{2}+\frac{w_0}{2}}\right)^2} \quad (14)$$

where $T_r(x,t)$ is the temperature of the filament that evolves with time.

Once the evolution of sintering angle is known, the evolution of the neck radius $y(t)$ with time can be obtained as

$$y(t) = \frac{H_0}{2}\sin(\theta(t)) \quad (15)$$

This model was numerically implemented in Matlab, where the integration method Runge-Kutta-Fehlberg was used to solve the differential Eq. (14).

3.3. Thermal-sintering coupling

In the original model proposed by Costa et al. [23], the perimeter of the filament cross-section as well as the contact fraction are assumed constant during the printing process. However, these evolve with the sintering process. Therefore, both thermal and sintering models are fully coupled as follows: (*i*) the thermal part of the model calculates the temperature of the filament segments $T_r(x,t)$ taking into account the contacts between them and with the support; (*ii*) this calculated temperature is used by the sintering part of the model to compute the sintering necks between filament segments $y(t)$; (*iii*) the computed sintering necks are used to determine the updated contacts between filaments and support $\lambda_{ri}(x,t)$ in the thermal part of the model.

In this regard, we consider that when the deposition of a new layer begins, the temperature of the previous layer is far below the critical sintering temperature and, thus, the sintering process between layers does not take place any longer. In other words and according to Fig. 4, the sintering process can take place between each filament segment and their contacts 2 and 4, while the process for contacts 1 and 3 can be neglected. The different expressions for the perimeter of the filament segment and the contact fraction evolution can be found in *Supplementary Information* (*Section S4*).

However, as stated before, one simplification of the model may consider the fraction contact perimeter as a constant, allowing to significantly reduce computational costs. With the aim of evaluating the suitability of this simplification, we performed a comparative study of the simulations provided by this approach and the results provided by the full model. The comparison of both approaches can be found in *Supplementary Information* (*Section S5*). The differences between both are lower than 2% in terms of angle of intersection. Therefore, we assume this simplification hereafter to avoid unnecessary high computational cost.

4. Modelling of the mesostructure of FDM components and theoretical predictions of mechanical properties

The two-stage thermo-structural model presented in the previous section allows for the simulation of the bonding process as well as for the prediction of the final geometry of the mesostructure. The void density can be easily determined from the final geometry of the filaments and their arrangement. These structural characteristics, together with the properties of the material, determine the mechanical performance of the final FDM component and, in particular, the Young's modulus and maximum stress reached. In this section, the void density (i.e., porosity) and the resulting mechanical properties are derived through analytical expressions making use of the outputs of the two-stage model.

4.1. Analytical modelling for void density estimation

The void density is defined as the ratio of the area of voids to the cross-sectional area. Assuming that the sintering process is symmetric, only half of each adjacent filament is considered, see Fig. 6a, where $\delta = \frac{H_0}{2}\cos(\theta(t))$.

The void density can thus be calculated from experimental measurements of the neck diameter and width as

$$\rho_{voids} = \frac{{H_0}^2\cos(\theta(t)) - \left[\pi\left(\frac{H_0}{2}\right)^2 - \left(\frac{H_0}{2}\right)^2(2\theta(t) - \sin(2\theta(t)))\right]}{H_0 w(t) + {H_0}^2\cos(\theta(t))} \quad (16)$$

A comparison between experimental results and analytical prediction can be found in *Supplementary Information* (*Section S6*).

4.2. Analytical modelling for mechanical properties estimation

The main challenge in FDM is the determination of the influence of the printing parameters on the mechanical properties. Numerous semi-analytical and theoretical relationships have been proposed in the literature to determine the dependence of mechanical properties on porosity. These equations are usually classified into linear, power or exponential mechanical properties-porosity relationships [31]. In this subsection, phenomenological expressions for the Young's modulus and maximum stress are proposed as a function of two structural parameters: the number of layers Z and the void density ρ_{voids}. The choice of these analytical expressions was motivated by the following points. They first need to be consistent with the limit cases of no voids and no polymeric material. In this regard, if ρ_{voids} is equal to zero (perfect bonding), the values of Young's modulus and maximum stress must be the properties of the virgin material. Conversely, if ρ_{voids} is equal to 1 (100%), i.e., no material, the values have to be

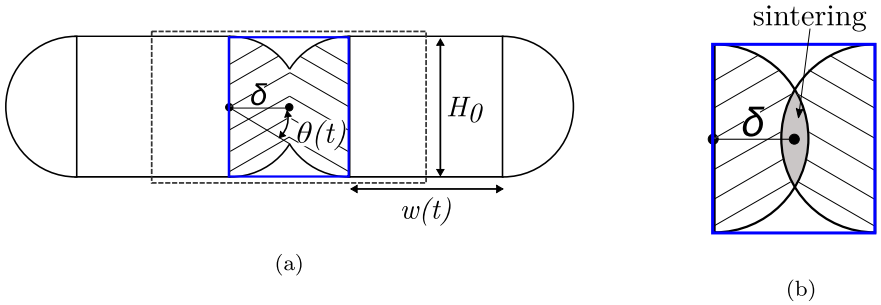

Fig. 6. Final cross-section geometry of a filament.

zero. Secondly, as informed by the experimental results, a linear tendency with the void density can be observed (defined by the printing parameters) while an asymptotic tendency is expected as the number of layers increases. The proposed formulations are defined here so as to fulfill these requirements while simplifying their analytical form. According to these assumptions, analytical expressions for the polymeric mechanical properties for longitudinal raster orientation are chosen as

$$\begin{aligned} E_{long} &= E_{01}\left(e^{\left[(1-\rho_{voids})^{C_E}\, Z\right]} - \rho_{voids}\right) + E_{02}\,(1-\rho_{voids}) \\ \sigma_{long} &= \sigma_{01}\left(e^{\left[(1-\rho_{voids})^{C_{1\sigma}}\, Z^{C_{2\sigma}}\right]} - \rho_{voids}\right) + \sigma_{02}\,(1-\rho_{voids}) \end{aligned} \tag{17}$$

where E_{01}, E_{02}, σ_{01} and σ_{02} are material parameters related to the Young's modulus and maximum stress. These parameters are constrained by the condition that $E_{long} = E_{01}e + E_{02}$ and $\sigma_{long} = \sigma_{01}e + \sigma_{02}$, corresponding to the values specified in the datasheet of the ABS filament respectively. The parameters C_E and $C_{1\sigma}$ control the sensitivity of the mechanical properties with respect to the number of layers, and need to be calibrated from experimental results. Finally, $C_{2\sigma} = \pm 1$ controls the sign of the asymptotic tendency experimentally observed by the maximum stress with the number of layers for each raster orientation. In addition, if the number of layers tends to infinity, the mechanical properties are $E_{long} = (E_{01} + E_{02})(1-\rho_{voids})$ and $\sigma_{long} = (\sigma_{01} + \sigma_{02})(1-\rho_{voids})$, respectively.

Regarding the properties for transverse raster orientation, they can be obtained as a multiple of the longitudinal ones by making use of empirical factors ζ such that

$$\begin{aligned} E_{trans} &= \zeta_1 E_{long} \\ \sigma_{trans} &= \zeta_2 \sigma_{long} \end{aligned} \tag{18}$$

The material parameters were calibrated (using the Matlab function *fminsearch*) against the experimental results of FDM ABS. The optimised parameters are shown in Table 2.

5. Results and discussion

5.1. End-to-end simulations of the printing process

The methodology proposed in this work is used to predict the final characteristics of FDM components (see Fig. 2). First, specific material and printing parameters are taken as inputs for the thermo-structural model, in turn providing the temperature evolution of each filament. Once the evolution of the filament temperature has been obtained, this is taken as input to predict the neck growth between filaments. At this stage, the void density can be predicted from the final geometry of the filaments using the theoretical expression in Eq. (16).

We provide in *Supplementary Information* (*Table S7*) the model predictions of the void densities computed for the different configurations used in this work. In addition, details on the model parameters used in these simulations are provided in *Supplementary Information* (*Section S7*). Although the present model is able to predict all the qualitative tendencies between printing parameters and resultant void density, it still needs further development to faithfully reproduce the full printing process. In this regard, the model proposed assumes a symmetric shape and the same temperature distribution inside the filament cross-section. Furthermore, the two-stage model does not consider the pressure of the extruder during the material deposition or the asymmetric temperature distribution inside the cross-section of the filaments [10]. These effects result in an asymmetric shape of the bond between filaments and a flattening on the top of filaments (see Fig. 3). These specific aspects must be addressed in future work to provide more accurate results.

Finally, the mechanical properties can be predicted from the void density estimations and the mechanical properties of the virgin FDM ABS. These results (model predictions) are compared against the experimental data in Fig. 7 (results for a transverse raster orientation are shown in *Supplementary Information, Fig. S6*). The model captures the different trends as a function of the void density and layer height with an error smaller than 14%. The only case of study with a larger error than 14% is the prediction of the elastic modulus for the longitudinal three-0.1 mm-layer specimen. This result can be explained by an overestimation of the void density.

Although the methodology proposed in this work has only been applied to FDM ABS, the formulation of the model permits its application to other thermoplastics. To do so, one would need to identify first the material properties used as input data in the model (according to Fig. 2): thermal properties, viscosity, surface tension

Table 2
Model parameters for theoretical modelling of mechanical properties.

C_E	$C_{2\sigma Long}$	$C_{2\sigma Trans}$	$C_{1\sigma}$	E_{01} (MPa)	E_{02} (MPa)	σ_{01} (MPa)	σ_{02} (MPa)	ζ_1	ζ_2
23	1	−1	21	318	1497	6	31	0.94	0.45

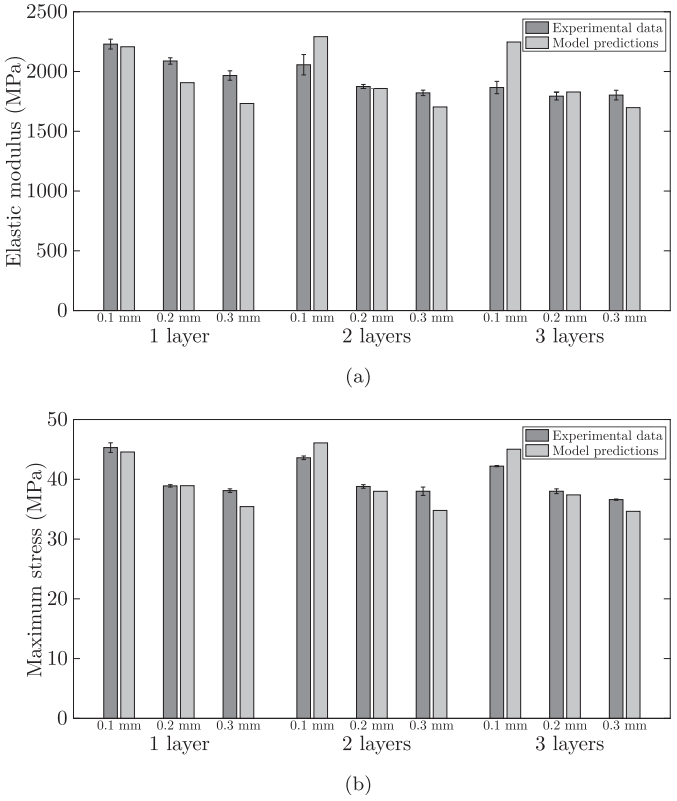

Fig. 7. Comparison between experimental mechanical properties (with error bars) and predictions for longitudinal specimens.

and the mechanical properties of the virgin material. These material properties along with printing parameters can be used as input to provide the mesostructural features of the printed component. To complete the framework and provide the final mechanical properties, characterisation tests on the specific material are needed to calibrate the parameters of the analytical expressions.

This proposed methodology allows for the prediction of the heterogeneous porosity distribution within the printed component as a result of thermal spatial gradients during the manufacturing process. However, to reduce computational cost and without loss of generality, we have assumed a representative filament-to-filament condition to provide a homogenised component porosity as a first approximation. This limitation can be overcome in future work by increased computation efficiency, e.g., by parallelisation of the code.

5.2. Parametric study of the influence of printing and process parameters

The methodology proposed in this work allows for the simulation of the bonding process during printing and the estimation of void density and mechanical performance of a specific FDM polymeric component depending on the printing and process parameters. It is consequently possible to find the optimal parameters to obtain a specific set of mechanical properties depending on the final application. Note that if the choice of the printing parameters is not aligned with the recommended working conditions, the temperature within the filaments can, for example, rapidly decrease below the glass transition, interrupting the sintering process. This will result in a poor angle of intersection suggesting a bad quality of the component. For example, by decreasing the extrusion and environment temperature, one can observe (both numerically and experimentally) a bad adhesion between filaments leading to poor mechanical properties. Thus, while the proposed model is not *per se* designed to identify the recommended working conditions, it can still offer insights into which conditions should not be acceptable.

Thus, in order to show the potential of the methodology proposed, a parametric study of the influence of printing and process parameters on the mesostructural and mechanical properties of the FDM ABS has been developed in this section. The reference parameters are chosen to be the ones used in the previous subsection for a longitudinal specimen with two layers with heights of 0.3 mm. The results in terms and mechanical properties are shown in Fig. 8 (the results in terms of void density can be found in the *Supplementary Information, Fig. S7*).

The model results show that the parameter with the greatest influence is the layer height, decreasing the void density by more than 97% when the layer height goes from 0.3 to 0.1 mm. In addition, higher environmental or support temperature lead to lower void densities. In this regard, note that for an environmental temperature of 90 °C, near the support temperature (100 °C), the void density decreases by up to 53%. Finally, when the printing speed is increased, the percentage of voids density slightly decreases. However, although the manufacturing time and void density decrease, a loss of dimensional accuracy is expected when the printing speed is increased.

As all the cases simulated have two layers, higher mechanical properties are obtained for those with lower void density. Thus, considering the reference layer height (0.3 mm), the elastic modulus and the maximum stress both increase by 9% in average for a decrease of layer height to 0.2 mm, and 33% in average for a decrease of layer height to 0.1 mm. These tendencies are in qualitative agreement with the experimental results (see *Supplementary Information, Table S3*) where the elastic modulus and maximum stress increase by 3% and 2%, respectively, when the layer height changes from 0.3 mm to 0.2 mm, and by 13% and 14% when the layer height changes from 0.3 mm to 0.1 mm. Moreover, following the same tendency observed

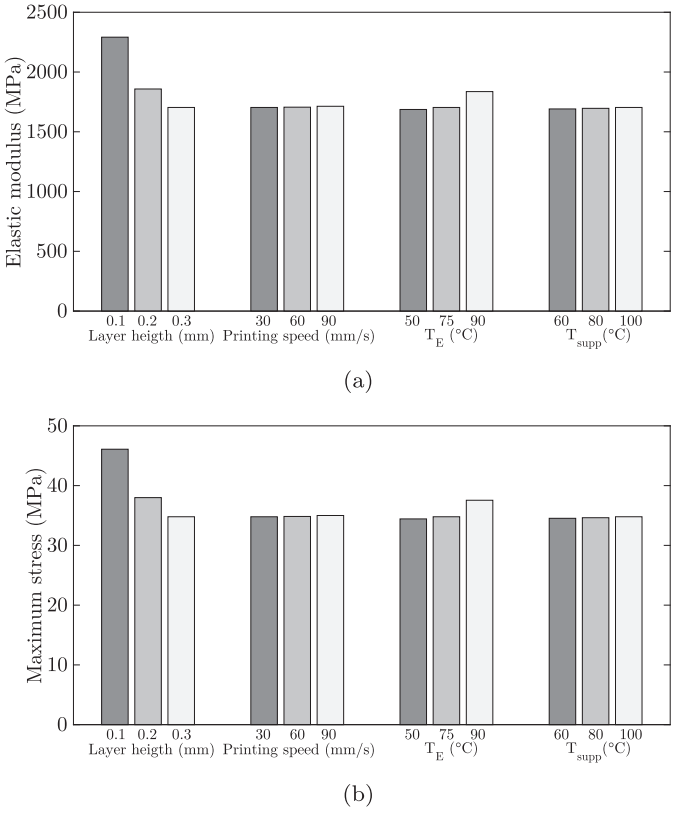

Fig. 8. Influence of printing and process parameters in the mechanical properties.

for void density, the mechanical properties increase by up to 7% for an increase of environmental temperature of 90 °C.

6. Conclusions

In this work, a new modelling methodology was presented for the prediction of the mechanical performance of FDM components. This modelling tool makes use of manufacturing parameters and filament properties and outputs the mechanical properties and mesostructure of the printed components.

First, an experimental characterisation was carried out to study the influence of three printing parameters on the void density and mechanical performance of ABS components: layer height, raster orientation and number of layers. Higher elastic modulus and maximum stress are observed for lower layer heights and longitudinal raster orientation. This improvement is accompanied by a decrease in the void density. Moreover, increasing the number of layers leads to lower mechanical properties, with the exception of the maximum tension for transverse components.

A new implementation of the thermal model developed by Costa et al. [23] was presented to predict the temperature evolution of filaments. In addition, a new sintering model was developed by considering a filament geometry based on experimental observations. The two-stage model allows for the estimation of the final cross-sectional geometry of filaments.

Moreover, theoretical expressions were developed to predict the void density and mechanical properties taking as inputs manufacturing parameters, filament properties and outputs from the thermal and sintering models. The model predictions reproduce the tendencies observed in experimental results.

Finally, a parametric study was conducted to illustrate the potential of the proposed model for the optimisation of FDM components. This study points to the layer height and environment temperature as the most relevance manufacturing parameters.

CRediT authorship contribution statement

S. Garzon-Hernandez: Investigation, Methodology, Formal analysis, Writing - original draft, Writing - review & editing. **D. Garcia-Gonzalez:** Investigation, Methodology, Formal analysis, Writing - review & editing. **A. Jérusalem:** Methodology, Formal analysis, Writing - review & editing. **A. Arias:** Investigation, Formal analysis, Writing - review & editing.

Declaration of competing interest

The authors declare that they have no known competing financial interests or personal relationships that could have appeared to influence the work reported in this paper.

Acknowledgments

D. Garcia-Gonzalez acknowledges support from the Talent Attraction grant (CM 2018 - 2018-T2/IND-9992) from the Comunidad de Madrid. S. Garzon-Hernandez, D. Garcia-Gonzalez and A. Arias acknowledge support from Ministerio de Ciencia, Innovación y Universidades, Agencia Estatal de Investigación y Fondo Europeo de Desarrollo Regional, como entidades financiadoras (RTI2018-094318-B-I00).

Appendix A. Supplementary data

Supplementary data to this article can be found online at https://doi.org/10.1016/j.matdes.2019.108414.

References

[1] T.D. Ngo, A. Kashani, G. Imbalzano, K.T. Nguyen, D. Hui, Additive manufacturing (3D printing): a review of materials, methods, applications and challenges, Compos. Part B 143 (2018) 172–196. http://www.sciencedirect.com/science/article/pii/S1359836817342944.
[2] Y. Kim, H. Yuk, R. Zhao, S.A. Chester, X. Zhao, Printing ferromagnetic domains for untethered fast-transforming soft materials, Nature 558 (2018) 274–279.
[3] D. Garcia-Gonzalez, Magneto-visco-hyperelasticity for hard-magnetic soft materials: theory and numerical applications, Smart Mater. Struct. (2019) http://iopscience.iop.org/10.1088/1361-665X/ab2b05.
[4] J. Chacón, M. Caminero, E. García-Plaza, P. Núñez, Additive manufacturing of PLA structures using fused deposition modelling: effect of process parameters on mechanical properties and their optimal selection, Mater. Des. 124 (2017) 143–157. http://www.sciencedirect.com/science/article/pii/S0264127517303143.
[5] C. Bellehumeur, L. Li, Q. Sun, P. Gu, Modeling of bond formation between polymer filaments in the fused deposition modeling process, J. Manuf. Process. 6 (2) (2004) 170–178. http://www.sciencedirect.com/science/article/pii/S1526612504700717.
[6] F. Bahr, E. Westkamper, Correlations between influencing parameters and quality properties of components produced by fused deposition modeling, Procedia CIRP 72 (2018) 1214–1219. 51st CIRP Conference on Manufacturing Systems. http://www.sciencedirect.com/science/article/pii/S2212827118301483.
[7] Q. Sun, G. Rizvi, C. Bellehumeur, P. Gu, Effect of processing conditions on the bonding quality of FDM polymer filaments, Rapid Prototyp. J. 14 (2) (2008) 72–80. https://doi.org/10.1108/13552540810862028.
[8] C.T. Bellehumeur, M.K. Bisaria, J. Vlachopoulos, An experimental study and model assessment of polymer sintering, Polym. Eng. Sci. 36 (17) (1996) 2198–2207. 2207https://onlinelibrary.wiley.com/doi/abs/10.1002/pen.10617.
[9] O. Pokluda, C.T. Bellehumeur, J. Vlachopoulos, Modification of Frenkel's model for sintering, AIChE J. 43 (12) (1997) 3253–3256. https://onlinelibrary.wiley.com/doi/abs/10.1002/aic.690431213.
[10] J.F. Rodriguez, J.P. Thomas, J.E. Renaud, Characterization of the mesostructure of fused-deposition acrylonitrile-butadiene-styrene materials, Rapid Prototyp. J. 6 (3) (2000) 175–186. https://doi.org/10.1108/13552540010337056.
[11] L. Li, Q. Sun, C. Bellehumeur, P. Gu, Composite modeling and analysis for fabrication of FDM prototypes with locally controlled properties, J. Manuf. Process. 4 (2) (2002) 129–141. http://www.sciencedirect.com/science/article/pii/S1526612502701394.
[12] J. Rodriguez, J. Thomas, J.E. Renaud, Design of fused-deposition ABS components for stiffness and strength, J. Mech. Des. 125 (3) (2003) 545.–551.
[13] A.K. Sood, R. Ohdar, S. Mahapatra, Parametric appraisal of mechanical property of fused deposition modelling processed parts, Mater. Des. 31 (1) (2010) 287–295. http://www.sciencedirect.com/science/article/pii/S0261306909002945.
[14] A.K. Sood, R.K. Ohdar, S.S. Mahapatra, Experimental investigation and empirical modelling of FDM process for compressive strength improvement, J. Adv. Res. 3 (1) (2012) 81–90. http://www.sciencedirect.com/science/article/pii/S209012321100066X.
[15] N. Aliheidari, R. Tripuraneni, A. Ameli, S. Nadimpalli, Fracture resistance measurement of fused deposition modeling 3D printed polymers, Polym. Test. 60 (2017) 94–101. http://www.sciencedirect.com/science/article/pii/S0142941817300065.
[16] A.R. Torrado, D.A. Roberson, Failure analysis and anisotropy evaluation of 3D-printed tensile test specimens of different geometries and print raster patterns, J. Fail. Anal. Prev. 16 (1) (Feb 2016) 154–164. https://doi.org/10.1007/s11668-016-0067-4.
[17] B. Rankouhi, S. Javadpour, F. Delfanian, T. Letcher, Failure analysis and mechanical characterization of 3D printed ABS with respect to layer thickness and orientation, J. Fail. Anal. Prev. 16 (3) (Jun 2016) 467–481. https://doi.org/10.1007/s11668-016-0113-2.
[18] J.F. Rodríguez, J.P. Thomas, J.E. Renaud, Mechanical behavior of acrylonitrile butadiene styrene (ABS) fused deposition materials. Experimental investigation, Rapid Prototyp. J. 7 (3) (2001) 148–158. https://doi.org/10.1108/13552540110395547.
[19] S. Ahn, M. Montero, D. Odell, S. Roundy, P.K. Wright, Anisotropic material properties of fused deposition modeling ABS, Rapid Prototyp. J. 8 (4) (2002) 248–257. https://doi.org/10.1108/13552540210441166.
[20] C. Ziemian, M. Sharma, S. Ziemian, Anisotropic mechanical properties of ABS parts fabricated by fused deposition modelling, in: M. Gokcek (Ed.), Mechanical Engineering, IntechOpen, Rijeka, 2012, Ch. 7. https://doi.org/10.5772/34233.
[21] R. Zou, Y. Xia, S. Liu, P. Hu, W. Hou, Q. Hu, C. Shan, Isotropic and anisotropic elasticity and yielding of 3D printed material, Compos. Part B 99 (2016) 506–513. http://www.sciencedirect.com/science/article/pii/S1359836816309052.
[22] ImageJ, (2019) https://imagej.nih.gov/ij/.
[23] S. Costa, F. Duarte, J. Covas, Estimation of filament temperature and adhesion development in fused deposition techniques, J. Mater. Process. Technol. 245 (2017) 167–179. http://www.sciencedirect.com/science/article/pii/S0924013617300791.
[24] J. Thomas, J. Rodriguez, Modeling the fracture strength between fused-deposition extruded roads, Proc. Solid Freeform Fabr. Symp (2000) 16–23.
[25] S. Costa, F. Duarte, J. Covas, Thermal conditions affecting heat transfer in FDM/FFE: a contribution towards the numerical modelling of the process, Virtual Phys. Prototyping 10 (1) (2015) 35–46. https://doi.org/10.1080/17452759.2014.984042.

[26] R.S. Palais, R.A. Palais, Differential Equations, Mechanics, and Computation, 51. American Mathematical Soc. 2009.
[27] N. Rosenzweig, M. Narkis, Sintering rheology of amorphous polymers, Polym. Eng. Sci. 21 (1981) 1167–1170.
[28] J. Frenkel, Viscous flow of crystalline bodies under the action of surface tension, J. Phys. 9 (1945) 385–391.
[29] J. Eshelby, Discussion of 'Seminar on the Kinetics of Sintering', Metall. Trans 185 (1949) 796–813.
[30] R.W. Hopper, Coalescence of two equal cylinders: exact results for creeping viscous plane flow driven by capillarity, J. Am. Ceram. Soc. 67 (12) (1984) C262–C264. https://ceramics.onlinelibrary.wiley.com/doi/abs/10.1111/j.1151-2916.1984.tb19692.x.
[31] J.A. Choren, S.M. Heinrich, M.B. Silver-Thorn, Young's modulus and volume porosity relationships for additive manufacturing applications, J. Mater. Sci. 48 (15) (Aug 2013) 5103–5112. https://doi.org/10.1007/s10853-013-7237-5.